 doi:10.20944/preprints201809.0536.v1

*Article*

# Improvement of Tubular Permanent Magnet Machine Performance Using Dual-Segment Halbach Array

**Minh-Trung Duong [1,2], Yon-Do Chun [1,2]**

[1] Energy and Power Conversion Engineering, University of Science and Technology; Duong.MT@keri.re.kr
[2] Electric Motor Research Center, Korea Electrotechnology Research Institute; Ydchun@keri.re.kr
* Correspondence: Ydchun@keri.re.kr; Tel.: +82-055-280-1490

**Abstract:** In this paper, modification of dual-Halbach permanent magnet (PM) array is investigated to improve performance of tubular linear machine, in terms of flux density and output power. Instead of a classical Halbach array with only radial and axial PMs, proposed model involves insertion of mig-magnets, which have magnetized angle shifted from the reference magnetized angles of axial and radial PMs. This structure leads to elimination of flux leakage and concentration of flux linkage in middle of the coil; therefore, the performance of machine is increased.

**Keywords:** electromagnetic shock absorber, tubular machine, energy harvesting, Halbach array.

## 1. Introduction

Tubular machine are commonly applied in many industrial applications, such as cryocoolers, linear compressors, or refrigerators [1–3]. Recent research activities for energy harvesting in vehicle suspension systems [4] or using ocean wave energy [5] have proposed the new trend for the tubular machines. From a design viewpoint, at a particular volume, the increase of the output power is very difficult. L. Zou *et al.* [6] provide the original design, which is composed of one magnet layer using a Halbach arrangement instead of only axial magnets or radial magnets array. In the following step, by using the same Halbach array structure, X. Tang *et al.* [7] modified the original model with a double layer of permanent magnet; this method eliminates the flux leakage, while flux density in the middle of the coil is concentrated. This leads to an eightfold improvement of the output power and a 3.8 times improvement of the power density compared to those values of the original design.

Another technique was studied by Y. Shen, in which mid-magnets of which the magnetization angle is shifted from the reference angle of axial and radial magnets are inserted [8]. There are two possible structures, including odd-segment or even-segment, and these structures define the number of magnet segments over a pole pitch as an odd or even number. The FEM and analytical results for a 12-slot/ 10-pole PM brushless machine illustrate that the 3-segment Halbach array exhibits significantly higher fundamental airgap flux density than of the magnet cylinder having a traditional Halbach array with two segments. Under the same theory, W. Zhao designed a linear generator for energy harvesting from body motion [9] using an even-segment Halbach array. The eight-segment dual Halbach array is employed in the optimized generator because its magnetic flux density is greater than that of the four-segment array.

Preprints (www.preprints.org) | NOT PEER-REVIEWED | Posted: 27 September 2018 doi:10.20944/preprints201809.0536.v1

In this paper, a larger model assembled with a vehicle suspension system was designed based on the proposed segment-magnet dual Halbach array. The analysis results show that under the same operating conditions, the generator with the cylinder segment magnet yeilds higher output power than that of the generator with original Halbach array structure.

## 2. Tubular machine with classical Halbach array

### *2.1. Design specifications*

This section deals with the design specification of the tubular machine using classical Halbach array based on the actual dimensions of a commercial shock absorber in an SUV-Korando car. Analyses using FEM are validated by corresponding experiments.

Figure 1 shows the cross-section of the half model and its geometry over one pole pitch, as was presented in [10]. The overlapping length of the magnet array and coil windings is about 200 mm but, fortunately, this value is adjustable by ± 40 mm. That is also the condition for the outer diameter, which can be flexibly chosen at values between 80 mm and 160 mm, while the inner diameter has to be at least 40 mm, the same as the diameter of the damping part or the mechanical part [10].

Due to the relative position between the coils and the excited flux density, and with the desire to simplify the drive system, an external circuit is designed with two phases, in which phase 1 is in series connection with coil 1 and coil 3, phase 2 is in series connection with coil 2 and coil 4. It is mandatory to exactly set up the winding directions to achieve maximum power [6,10].

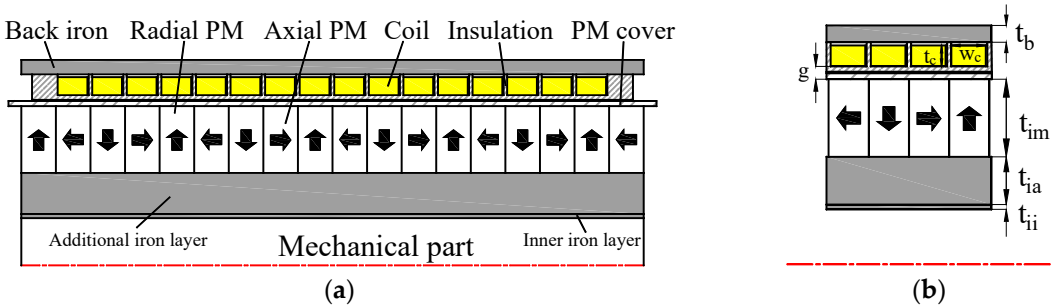


**Figure 1.** Half cross-section of the single PM layer coreless model

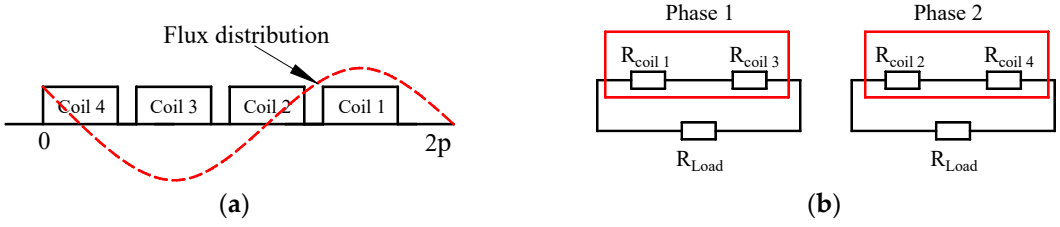


**Figure 2.** (**a**) Coils & excited flux density; (**b**) External circuit

The relative position between the coils and excited flux, and the external circuit, are shown in the Figure 2. According to [6,10,11] the maximum output power occurs at the maximum vibrating speed $v_{max}$ when the load resistance $R_L$ equals the sum of the coil resistance $R_c$; this is termed full load condition:

$$P_{max} = V_e I_0 = B_r^2 v_z^2 \sigma V_{coil} \quad (1)$$

where $V_{coil}$ is the coil volume.

Preprints (www.preprints.org) | NOT PEER-REVIEWED | Posted: 27 September 2018 doi:10.20944/preprints201809.0536.v1

Equation (1) shows that output power is proportional to the square of the radial flux density, square of the vibrating speed and the volumes of the coil. The relationship among the peak to peak stroke, the vibrating speed, and the vibrating frequency is calculated as follows:

$$\text{Stroke}_{\text{peak-to-peak}} = \frac{v_{max}}{\omega} = \frac{v_{rms}\sqrt{2}}{\pi f} \quad (2)$$

In addition, the instantaneous voltage of one coil centered at equilibrium position $z_0$ in the regenerative shock absorber is presented as a function of time, position, magnetic flux density, geometrical parameter, suspension velocity and frequency. For the 0° coil or for coil 1, which has maximum magnetic flux density, if the vibration amplitude is small, the voltage is calculated by:

$$V_{0^\circ} = B_0 L \left| \frac{j\omega}{\omega_n^2 - \omega^2 + 2j\zeta\omega_n\omega} e_{in} \right| \sin \omega t \quad (3)$$

and a 90° coil or coil 3 will have a double frequency wave:

$$V_{90^\circ} = B_0 L \frac{\pi V_{max}^2}{2H\omega} \sin 2\omega t \quad (4)$$

The additional iron layer is inserted to reduce the inner diameter of the PMs; this layer is composed of stainless steel, while the back iron is made of an electromagnetic material. Both radial PMs and axial PMs are made of DDP-40SH, which has relative flux density is $B_r$=1.26 T at 20°C and relative permeability of $\mu_r$=1.05. Windings are wound around and supported by a bobbin with a total number of turns per slot of 180.

Detailed specifications of the tubular machine are briefly summarized in Table 1.

**Table 1.** Design specifications of the tubular machine with classical Halbach array.

| Item | Value |
|---|---|
| Length, L (mm) | 243 |
| Outer diameter, D (mm) | 160 |
| PM thickness, $t_{im}$ (mm) | 26.0 |
| Radial PM width, $w_{rm}$ (mm) | 13.5 |
| Axial PM width, $w_{am}$ (mm) | 13.5 |
| Pole pitch, $\tau_p$ (mm) | 27.0 |
| Coil window thickness, $t_c$ (mm) | 8.0 |
| Coil window width, $w_c$ (mm) | 12.1 |
| Mechanical air gap, g (mm) | 4.3 |
| Inner iron thickness, $t_{ii}$ (mm) | 1.6 |
| Added iron thickness, $t_{ia}$ (mm) | 16.0 |
| Back iron thickness, $t_b$ (mm) | 5.6 |
| Wire diameter, $w_r$ (mm) | 0.6 |
| Number of winding/ slot, turns | 180 |
| Number of poles, $N_p$ | 8 |
| Number of slots, $N_s$ | 16 |
| Back iron material | S20C |
| PMs material | NdFeB – N40SH; $B_r$=1.26T (at 20°C); $\mu_r$=1.05 |

Preprints (www.preprints.org) | NOT PEER-REVIEWED | Posted: 27 September 2018 doi:10.20944/preprints201809.0536.v1

85 *2.2. Experimental verification of analysis*

86 According to [6], when a mid-size car is moving with 60 mph of speed on a road class C,
87 vibrating frequency on the shock absorber is estimated to be approximately 0.25 m/s. Under these
88 conditions, the peak to peak stroke length and vibrating frequency are about 11.25 mm and 10 Hz,
89 respectively. These conditions of the stroke length, vibrating speed, and linear frequency are
90 considered as a standard for the models studied in this paper. When applying the standard
91 conditions, the maximum and average power can be theoretically calculated at 76.09 W and 37.8 W,
92 respectively. To prepare for experimental verification, a prototype of a single layer coreless model
93 was fabricated and installed, as in the illustrations provided in Figures 3 and 4. Unfortunately, if the
94 linear frequency of the generator is 10 Hz, the required rotating speed of the sub-motor is 3000 rpm,
95 which exceeds the limitation of this motor; therefore, measurements were performed at lower
96 vibrating speeds.
97

98

99 **Figure 3.** Prototype

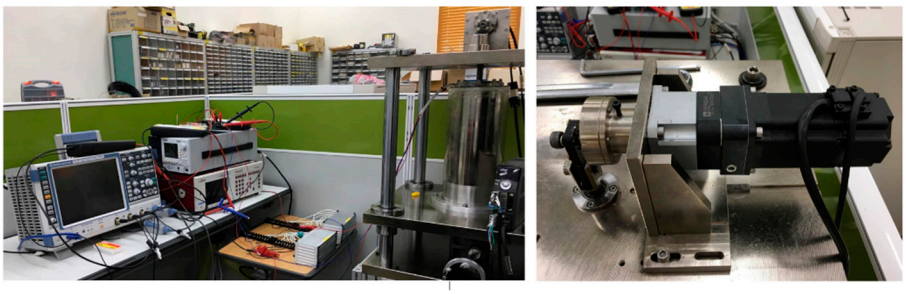

100

101 **Figure 4.** Experimental installment

102 With the assumption that the peak to peak stroke length is fixed at 11.25 mm, Figure 5 presents
103 the back EMF waveforms achieved for the load resistance when vibrating speed is 0.125 m/s, which
104 equals 50% of the standard. It can be clearly seen in the Figure 5(b) that the frequency of load 2 is
105 double that of load 1, which phenomenon can be predicted by Equations (3) and (4). Figure 6
106 illustrates the power variation according to various vibrating speeds under the full load condition.
107 While the maximum output voltage is well-matched between the analyses and the experiments, with
108 an average deviation of only 4.8%, the results of the average output power are not much satisfactory,
109 at around 13.5 %. It should be noted that although the resistance in one phase under full load
110 condition is measured at nearly 39.3 Ω, but in the experimental setup, only 39Ω of the load resistance
111 can be connected.

Preprints (www.preprints.org) | NOT PEER-REVIEWED | Posted: 27 September 2018 doi:10.20944/preprints201809.0536.v1

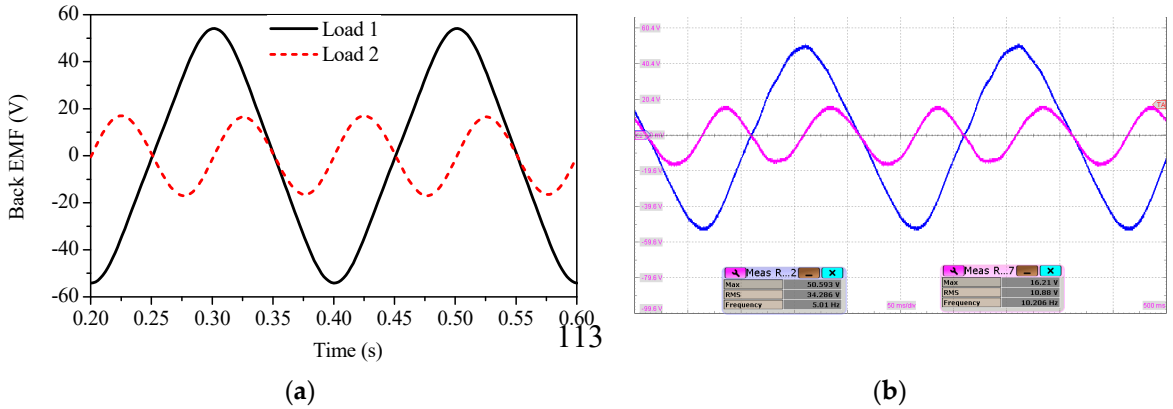


(**a**) (**b**)

**Figure 5**. Back EMF of the load resistors under 0.125 m/s of vibrating speed obtained from: (**a**) FEM analysis; (**b**) Experiment

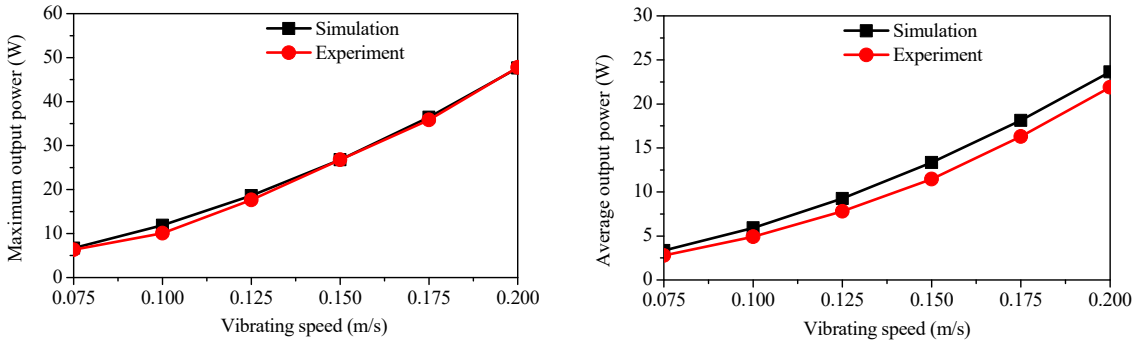


(**a**) (**b**)

**Figure 6.** Power variation according to vibrating speeds under full load condition: (**a**) maximum output power; (**b**) average output power

Figure 6 illustrates the power variation according to various vibrating speeds under the full load condition. While the maximum output voltage is well-matched between the analyses and the experiments, with an average deviation of only 4.8%, the results of the average output power are not much satisfactory, at around 13.5 %. It should be noted that although the resistance in one phase under full load condition is measured at nearly 39.3 Ω, but in the experimental setup, only 39 Ω of the load resistance can be connected.

Another noticeable phenomenon is the linear relationship between the output power and the square of the vibrating speed, according to Equation (1). For instance, when the generator is operating at 0.075 m/s, about 2.78 W of average power can be obtained. The average power under 0.15 m/s of vibrating speed can be predicted according to the following:

$$P_{0.15m/s} = P_{0.075m/s} \times \left(\frac{0.15}{0.075}\right)^2 = 2.78 \times \left(\frac{0.15}{0.075}\right)^2 \approx 11.12(W) \quad (4)$$

The measured result at 0.15 m/s of vibrating speed for average power is approximately 11.46 W, which is nearly the same as the expectation.

Preprints (www.preprints.org) | NOT PEER-REVIEWED | Posted: 27 September 2018 doi:10.20944/preprints201809.0536.v1

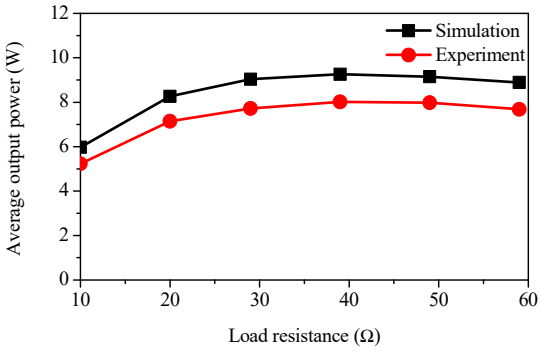


**Figure 7.** Average power according to various load resistances

Figure 7 illustrates the power variation according to various load resistances when the vibrating speed is 0.125 m/s and the peak to peak stroke length is 11.25 mm. Both the analysis and the experiment results present similar trends, with an average deviation of about 13.4%. When the load resistance equals the sum of the coil resistance, the average output power is at its maximum.

## 3. Tubular machine with novel Halbach array

In this section, a novel Halbach array is applied to the same tubular generator with the desire to improve the output power. Design specifications with the number of magnets, the sizes, and the magnetized direction are shown in Figure 8 and Table 2.

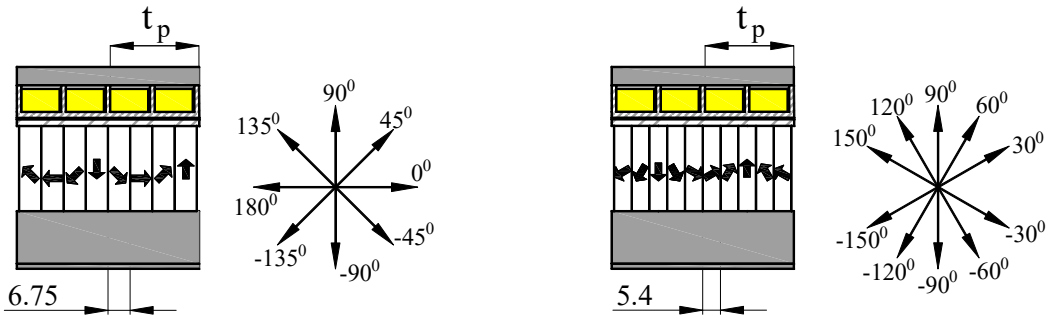


**Figure 8.** (**a**) 4-segment Halbach array; (**b**) 5-segment Halbach array

**Table 2.** Specifications of the magnet segments over one pole pitch

| Item | Classical Halbach array | 4-segment | 5-segment |
|---|---|---|---|
| Pole pitch, $\tau_P$ (mm) | | 27 | |
| Number of segments/ pole pitch | 2 | 4 | 5 |
| Width of each segment (mm) | 13.5 | 6.75 | 5.4 |
| Magnetized angle of mid-magnet | --- | 45° | 30° |

Based on the results in [8], instead of applying only axial and radial PMs over one pole pitch in a classical Halbach array, a number of mid-magnets with different magnetized angles are inserted. There are two applicable approaches, including even-segment, with an even number of magnets over one pole pitch, and odd-segment, with an odd number of magnets over one pole pitch. From the pole

Preprints (www.preprints.org) | NOT PEER-REVIEWED | Posted: 27 September 2018 doi:10.20944/preprints201809.0536.v1

pitch value, there are 4 magnet segments in the even-segment case and 5 magnet segments in the odd-segment case. For a fair comparison, the other dimensions such as length and diameter of the generator, the number of turns per slot, and the materials are the same for the 3 models.

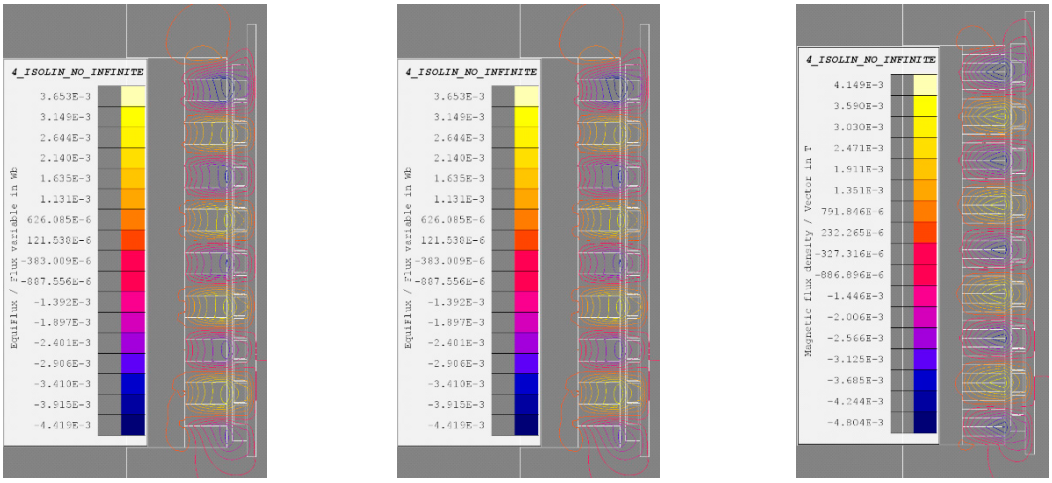


**Figure 9.** Flux distribution on the three different models under no-load condition: (**a**) classical Halbach array; (**b**) 4-segment; (**c**) 5-segment

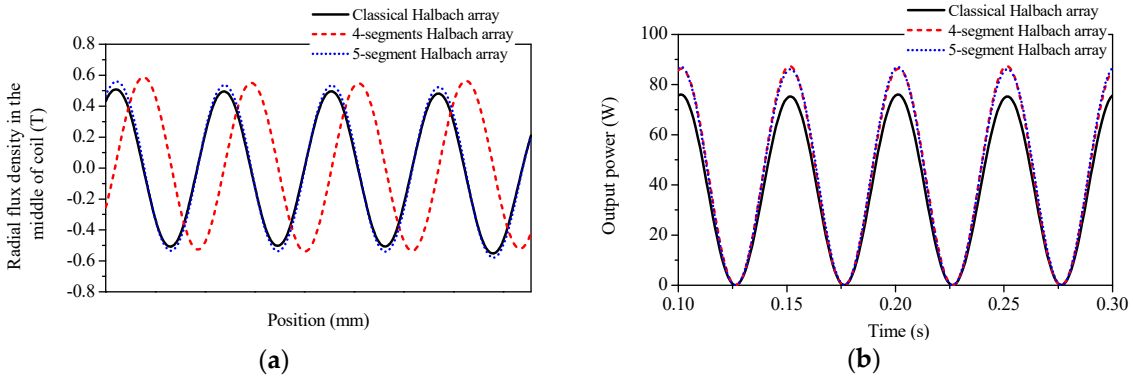


**Figure 10.** Comparison of the: (**a**) 4-segment Halbach array; (**b**) 5-segment Halbach array

**Table 3.** Comparison of three models

| Items | | Classical Halbach array | 4 segment | 5 segment |
|---|---|---|---|---|
| Vibrational speed, v (m/s) | | | 0.25 | |
| Stroke length (mm) | | | 11.25 | |
| Liner frequency f, (HZ) | | | 10 | |
| Radial flux density (T) | Max | 0.55 | 0.59 | 0.58 |
| | RMS | 0.36 | 0.39 | 0.39 |
| Maximum induced voltages (V) | Phase 1 | 54.10 | 57.98 | 57.86 |
| | Phase 2 | 17.05 | 18.53 | 19.12 |
| Output Power (W) | Max | 76.09 | 87.10 | 87.38 |
| | RMS | 37.78 | 43.53 | 43.47 |

Figure 9 shows the flux distribution on the 3 different models under a no-load condition, 0.25 m/s of vibrating speed, 11.25 mm of peak to peak stroke length and 10 Hz of linear speed. According to Equation (1), the output power is proportional to the radial flux density in the middle of the coil. In the cases of 4-segment and 5-segment magnet, the radial flux density increased by 6.8% and 5.2%, respectively; therefore, the output power can be expected to increase by around 15%. Figure 10 presents a comparison of the three models in terms of the radial flux density in the middle of the coil and the output power. The other characteristics are summarized in Table 3.

## 4. Conclusions

In this paper, a tubular permanent magnet machine composed of a novel magnet arrangement is proposed and compared with the conventional model in terms of radial flux density in the middle of coil and output power. A prototype of the tubular machine composed of the classical Halbach array was fabricated and validated with the FEM analyzed results, which show an average deviation of 13.5% in term of the output power.

Different from device using the classical Halbach array, the proposed model involves the insertion of mid-magnets, that have a magnetized direction that is shifted from that of the original axial and radial PMs. Based on FEM analyses, in the cases of 4-segment and 5-segment Halbach arrays, RMS values of the radial flux density increased by nearly 6.8%, which led to an increase of the average output power of 13.2%.

In further study, optimization of the relative dimensions and of the magnetized angle between the magnet segments will be performed.

**Acknowledgments:** This work was made possible by a grant from Civil-Military Technology Cooperation Program (No.: 16-CM-EN-17) funded by the Defense Acquisition Program Administration and the Ministry of Trade, Industry & Energy in Korea.

## References

1. Li, K.; Zhang, X.; Chen, H. Design Optimization of a Tubular Permanent Magnet Machine for Cryocoolers. *IEEE Transactions on Magnetics* **2015**, *51*, 1–8, doi:10.1109/TMAG.2014.2373337.
2. Wang, J.; Lin, Z.; Howe, D. Analysis of a short-stroke, single-phase, quasi-Halbach magnetised tubular permanent magnet motor for linear compressor applications. *IET Electric Power Applications* **2008**, *2*, 193–200, doi:10.1049/iet-epa:20070281.
3. Wang, J.; Howe, D.; Lin, Z. Design Optimization of Short-Stroke Single-Phase Tubular Permanent-Magnet Motor for Refrigeration Applications. *IEEE Transactions on Industrial Electronics* **2010**, *57*, 327–334, doi:10.1109/TIE.2009.2025710.
4. Shen, Y.; Lu, Q.; Ye, Y. Double-Stator Air-Core Tubular Permanent Magnet Linear Motor for Vehicle Active Suspension Systems. In *2016 IEEE Vehicle Power and Propulsion Conference (VPPC)*; 2016; pp. 1–6.
5. Cappelli, L.; Marignetti, F.; Mattiazzo, G.; Giorcelli, E.; Bracco, G.; Carbone, S.; Attaianese, C. Linear Tubular Permanent-Magnet Generators for the Inertial Sea Wave Energy Converter. *IEEE Transactions on Industry Applications* **2014**, *50*, 1817–1828, doi:10.1109/TIA.2013.2291939.

6. Design and characterization of an electromagnetic energy harvester for vehicle suspensions - IOPscience Available online: http://iopscience.iop.org/article/10.1088/0964-1726/19/4/045003/meta (accessed on Jun 4, 2018).
7. Tang, X.; Lin, T.; Zuo, L. Design and Optimization of a Tubular Linear Electromagnetic Vibration Energy Harvester. *IEEE/ASME Transactions on Mechatronics* **2014**, *19*, 615–622, doi:10.1109/TMECH.2013.2249666.
8. Shen, Y. Novel permanent magnet brushless machines having segmented Halbach array. phd, University of Sheffield, 2013.
9. Ma, C.; Zhao, W.; Qu, L. Design optimization of a linear generator with dual Halbach array for human motion energy harvesting. In *2015 IEEE International Electric Machines Drives Conference (IEMDC)*; 2015; pp. 703–708.
10. Duong, M.-T.; Chun, Y.-D.; Han, P.-W.; Park, B.-G.; Bang, D.-J.; Lee, J.-K. Design of An Electromagnetic Energy Harvesting System Applied to The Shock Absorber of A Sport Utility Vehicle Available online: http://www.dbpia.co.kr (accessed on Jun 4, 2018).
11. Goldner, R. B.; Zerigian, P. Electromagnetic linear generator and shock absorber 2005.